Icing Analysis of an Unprotected Aircraft Radome

J. Stone* and R. Ross†
Ross Aviation Associates, Sedgwick, Kansas

Artificial icing tests were conducted to determine the rate of ice accretion on an unprotected aircraft radome. These data are correlated with accepted means of calculating water catch rate. The theoretical method of calculating water catch rate is subsequently modified to produce a more accurate prediction technique. A method is also developed to predict the thickness distribution of the accumulated ice on the radome. Since fully descriptive icing tunnel data does not exist for radome shapes, assumptions are made concerning the shape of the forward fuselage in the determination of the average collection efficiency. Other assumptions, such as ice density and the amount of water catch that freezes, are made to give the highest ice accumulation.

Nomenclature

A	= frontal area, ft^2
a	= ellipsoid longitudinal semiaxis
b	= ellipsoid vertical semiaxis
c	= ellipsoid horizontal semiaxis
C.F.	= correlation factor
C_t	= thickness coefficient
D_D	= droplet diameter, μ
E_M	= water collection efficiency
E.T.	= elapsed time, h
h	= altitude, ft
K_0	= modified inertia parameter
K_2	= impingement parameter
KTAS	= knots true airspeed
LWC	= liquid water content, g/m^3
M	= water catch rate, lb/h
Re_D	= Reynolds number based on water droplet diameter
s	= reference length
S_U	= impingement limit to reference length ratio
T	= temperature, R
t	= ice thickness, in.
V	= velocity, KTAS
Vol.	= volume, ft^3
W	= water catch mass, lb
X	= limit of impingement, in.
λ/λ_s	= droplet range ratio
μ	= coefficient of viscosity, lb/(ft-s)
ρ	= air density, lb/ft^3

Subscripts

b	= bottom
n	= nose
s	= side
t	= top

Introduction

THE majority of experimental icing data was developed prior to 1960 with emphasis on airfoil/wing icing. The data presented for fuselage shapes tend to lack the necessary information for further application. Since the data presented for bodies-of-revolution are adequate for calculations, these are utilized as an approximation to the forward fuselage shape. Using the experimental data, correlations are made with the theoretical calculations and then carried one step further to predict the thickness distribution on the surface of the airplane radome.

Flights behind a tanker aircraft were performed using a Particle Measurement Systems, Inc., axially scattering probe and a cloud particle spectrometer to measure droplet diameter and liquid water content. No discussions of the instrumentation and experimental technique are contained in this report.

Measured Ice Accumulation

Data were used from four test flights to estimate radome ice accumulation. Photographs from each flight were examined and, using known dimensions on the forward fuselage, a scale factor was determined. By comparing the actual contours of the forward fuselage to the photographs, an ice thickness was measured for the upper and lower surface and the nose. (The lower surface thickness was also substantiated by the ice accumulation on an icing probe.) Since no plan view photographs were available, the ice thickness was estimated by using ¾ view photographs of the side of the fuselage. The volume of the forward fuselage was calculated without the ice accumulation by assuming an ellipsoid with semiaxes of a, b, and c, see Fig. 1. This assumption is substantiated later in the report.

The respective ice thickness was then added to each dimension and a new volume calculated, see Fig. 2. The difference in volume was used to calculate an approximate mass of accumulated ice. Table 1 presents the results of the above calculations.

Calculated Ice Accumulation

References 1 and 2 present methods for calculating ice accumulation for given flight conditions. However, the methods only apply to body shapes for which experimental data are available. For slender bodies, such as a fuselage, only bodies of revolution have adequate data presented in the above references to perform theoretical ice accumulation calculations.

To simulate the airplane forward fuselage, several ellipsoids (10, 20, and 40%) with various major axes lengths (from 34 to 500 in.) were investigated for contour matching. It was determined that a 20% ellipsoid with a major axis of 250 in. is a reasonable contour match. Figure 3 presents side and plan views of the 20% ellipsoid along with the forward fuselage. As can be seen, the contours closely match in the plan view and approximate the contours in the side view. The ellipsoid as shown in the side view is located −5 deg to the fuselage waterline, which results in a reasonable contour match to the upper surface. Since the fuselage angle of attack in flight is

Presented as Paper 82-0281 at the AIAA 20th Aerospace Sciences Meeting, Orlando, Fla., Jan. 11-14, 1982; submitted Jan. 22, 1982; revision received May 10, 1982.

*Engineering Specialist. Member AIAA.
†Director. Associate Fellow AIAA.

approximately +5 deg, the resultant angle of attack for the ellipsoid is 0 deg. This also conveniently matches the angle of attack for the experimental data that are presented for a 20% ellipsoid in Refs. 1 and 2.

To verify that the 20% ellipsoid is indeed an adequate approximation to the forward fuselage, the limit of impingement of the ice was calculated using the method outlined in Ref. 1 and shown later in this report. The calculated limit of impingement was then compared with measurements of photographs of the artificial icing flights. However, it should be noted that the impingement limit observed during the artificial icing tests is not defined by a straight fuselage cut, but was similar to the sketch of Fig. 2. This is probably due to angle of attack and fuselage shape causing a higher airspeed on the sides of the fuselage. Since the primary purpose is to predict a mass accumulation of ice, an average limit of impingement was estimated for comparison with the theoretical calculations. The results, Fig. 4, show excellent agreement and, thus, it is concluded that the 20% ellipsoid is an adequate representation of the airplane forward fuselage.

The method used to calculate the radome ice accumulation and limit of impingement is identical to that used in Refs. 1-3. Equations (1-8) present a summary of the equations required for the complete calculation procedure.

$$\mu = 7.475 \times 10^{-7} (T)^{1.5} / (T + 216) \tag{1}$$

$$\rho = \frac{39.7}{T[\exp(h/27710 - 0.098774h)]} \tag{2}$$

$$Re_D = 5.538 \times 10^{-6} \rho V D_D / \mu \tag{3}$$

If $Re_D \leq 200$,

$$\lambda/\lambda_s = 0.98 - 0.134 \ell n(Re_D) \tag{4a}$$

If $Re_D > 200$,

$$\lambda/\lambda_s = 0.74 - 0.0887 \ell n(Re_D) \tag{4b}$$

$$K_2 = 3.029 \times 10^{-12} V D_D^2 / \mu \tag{5}$$

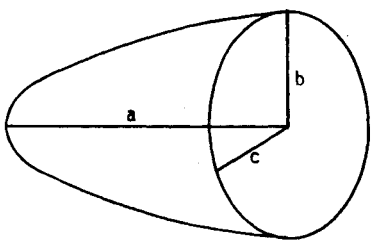

VOL = 2/3 π a b c

Fig. 1 Nose volume determination.

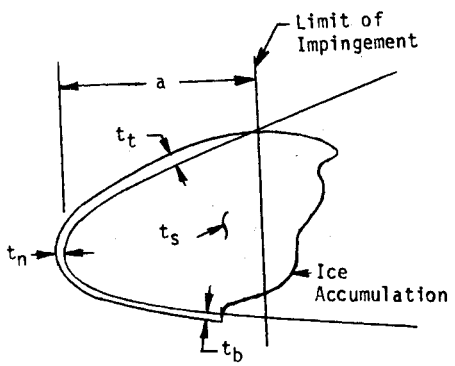

Fig. 2 Ice thickness.

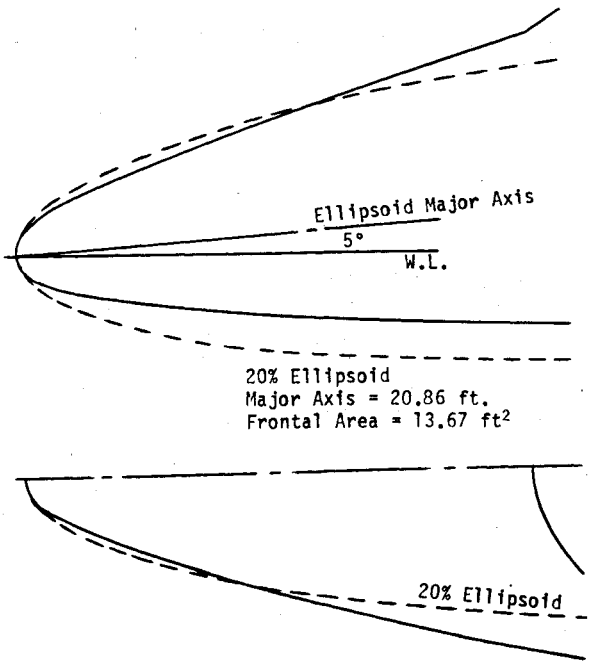

Fig. 3 Forward fuselage geometry.

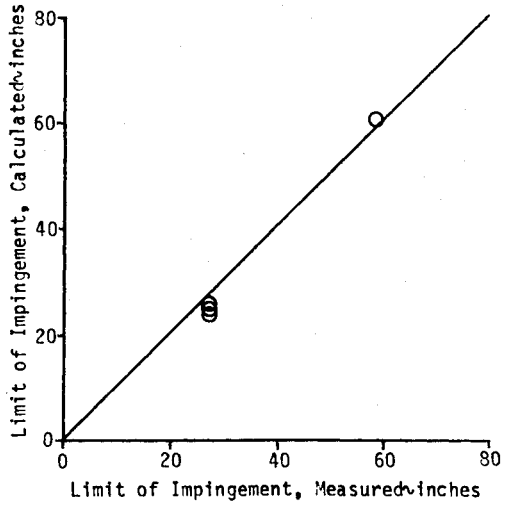

Fig. 4 Limit of impingement comparison.

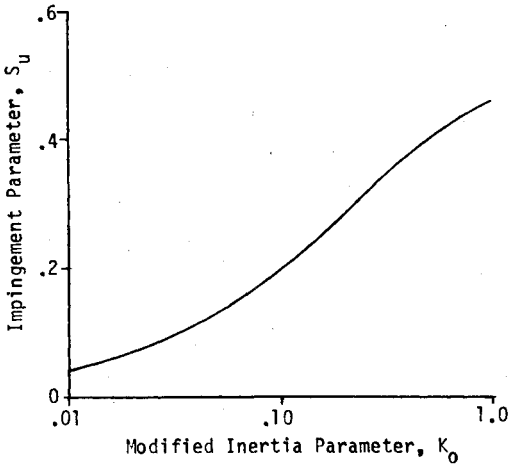

Fig. 5 Impingement parameter.

$$K_0 = (\lambda/\lambda_s)(K_2) \tag{6}$$

Reading S_U from Fig. 5, the impingement limit, inches aft of nose,

$$X = (s)(S_U) \tag{7}$$

Reading E_M from Fig. 6,

$$M = 0.38(A)(V)(\text{LWC})(E_M) \tag{8}$$

Figure 5 presents the limit of impingement parameter (S_U) and Fig. 6 presents the collection efficiency (E_M) for a 20% ellipsoid as shown in Refs. 1 and 2.

Results of theoretical calculations based on the flight conditions during the artificial icing tests are shown in Table 2. These calculations are based on the methods outlined in Eqs. (1-8).

Data Correlation

Data from both the artificial icing tests (Table 1) and the theoretical calculations (Table 2) are compared in Fig. 7. As can be seen, the ice accumulation during the artificial icing tests is greater than that predicted by theory. Several factors are present which explain this difference. Large droplet diameters and high liquid water contents may be outside the range of the theoretical calculations; the nosymmetrical shape of the forward fuselage and the fuselage being at an angle of attack, all would have a tendency to increase the water catch efficiency. It was determined that to predict the ice accumulation accurately, a correlation factor must be applied to the theoretical calculations. Using Fig. 7, a correlation factor of 4.285 was calculated. The results, shown in Fig. 8, show excellent agreement for the artificial icing flights available.

It should be noted that the previous data presented in this report do not include the correlation factor. To complete the calculations shown in Table 2, the water catch, M, Eq. (8) is multiplied by the correlation factor and elapsed time to produce the total expected water catch mass:

$$W = (M)(\text{C.F.})(\text{E.T.}) \tag{9}$$

Thickness Distribution

Using the data from the four artificial icing flights, a procedure has been developed for estimating the thickness distribution of the ice accumulation on the forward fuselage. Since the flight conditions were approximately the same for all three flights, the measured thicknesses, mass accumulations, and limits of impingement were averaged. Each average thickness was then multiplied by the ratio of limit of impingement to mass accumulation according to the following equation:

$$C_{t_x} = (X/W)\,t_x \tag{10}$$

This results in a set of coefficients suitable for estimating the accumulated ice thickness distribution:

Nose thickness coefficient:	$C_{t_n} = 0.260$ in.^{2}/lb
Side thickness coefficient:	$C_{t_s} = 0.551$ in.^{2}/lb
Top thickness coefficient:	$C_{t_t} = 0.405$ in.^{2}/lb
Bottom thickness coefficient:	$C_{t_b} = 0.300$ in.^{2}/lb

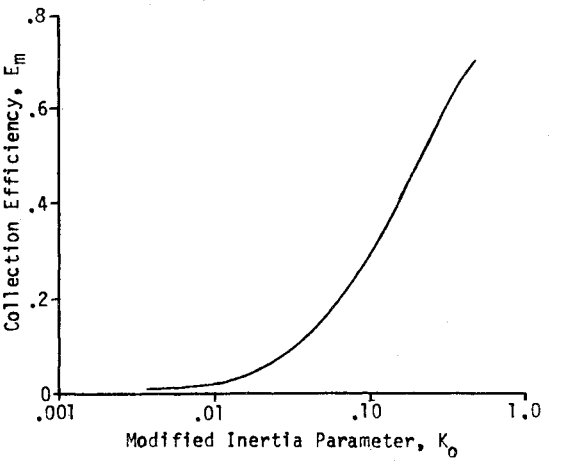

Fig. 6 Collection efficiency.

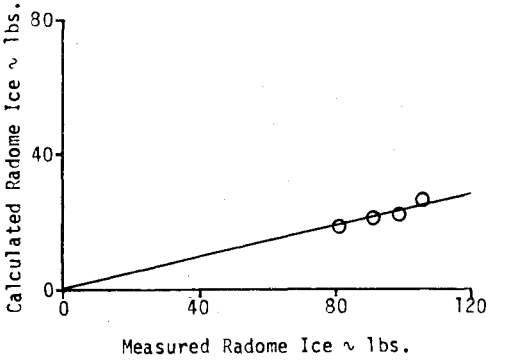

Fig. 7 Calculated vs measured ice accumulation.

Table 1 Measured radome ice accumulation

Flight	a, ft	b, ft	c, ft	t_n, in.	t_s, in.	t_t, in.	t_b, in.	a', ft	b', ft	c' ft	Δ vol., ft^3	w, lb
A	2.25	1.02	1.23	1.0	2.0	1.0	1.0	2.33	1.10	1.39	1.612	90.6
B	2.25	1.02	1.23	0.9	2.0	2.0	0.9	2.33	1.14	1.39	1.880	105.7
C	2.25	1.02	1.23	0.9	2.0	1.4	1.2	2.32	1.12	1.39	1.741	97.8
D	4.83	1.57	1.97	0.4	0.5	0.4	0.4	4.86	1.60	2.01	1.444	81.2

Table 2 Calculated radome ice accumulation

Flight	h, ft	T, °F	V, KTAS	D_D, μ	LWC, g/m^3	M, lb/h	Elapsed time, min.	W, lb
A	19,100	9.0	195	46	0.481	46.3	27	20.8
B	19,100	14.0	210	46	0.481	54.0	29	26.1
C	19,500	12.0	200	46	0.481	48.5	27	21.8
D	25,000	−10.0	260	99	0.08	41.7	26	18.1

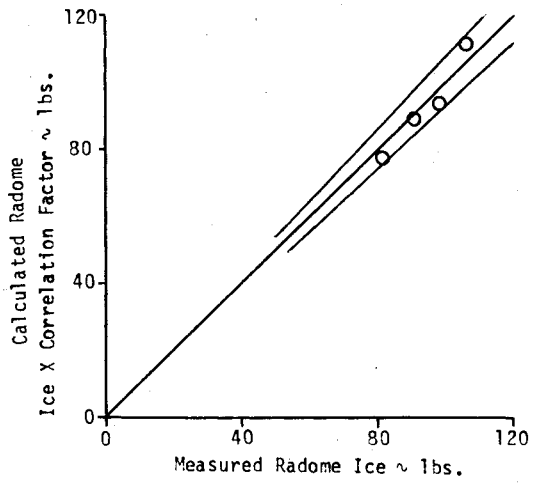

Fig. 8 Correlated ice accumulation.

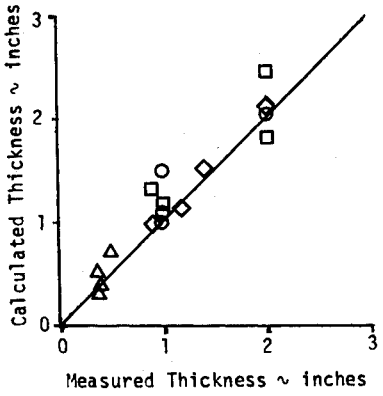

Fig. 9 Calculated vs measured ice thickness.

The thickness distribution can then be calculated by using these coefficients and the following equation:

$$T_x = (C_{t_x})\,(W/X) \tag{11}$$

where W and X are calculated by the methods of Eqs. (1-8).

Figure 9 presents a correlation of calculated and measured thickness. It is seen that, in general, the method derived is conservative in that it predicts thicker accumulations than are measured.

Conclusion

A method, based on experimental tests, has been derived to predict the limit of impingement, water catch rate, and ice thickness distribution for any icing and aircraft flight condition. Since there is no way to predict how much of the catch is actually accumulated as ice (especially for the near freezing temperatures), the assumption has been made that all the water catch freezes. The assumption has also been made that even though the accumulated ice appears irregular, the density is 56.2 lb/ft^3. Both assumptions will result in a conservative estimate of the accumulated ice.

The methods have been applied to the conditions as prescribed in FAR 25 Appendix C with successful results.

Acknowledgment

The authors express appreciation to the Gates Learjet Corporation for their cooperation in releasing the data for publication.

References

[1] Bowden, D.T., Gensemer, A.E., and Skeen, C.A., "Engineering Summary of Airframe Icing Technical Data," FAA ADS-4, March 1964.

[2] *SAE Aerospace Applied Thermodynamics Manual,* 2nd ed., Society of Automotive Engineers, Inc., New York, Oct. 1969.

[3] Heinrich, A., Ross R., and Ganesan, N., "Engine Inlet Anti-icing System Evaluation Procedure," FAA RD80-50, Jan. 1980.